A Pilot Study to Develop Paraneoplastic Cerebellar Degeneration Mouse Model

Fabrice Faure, Lidia Yshii, Toufic Renno, Isabelle Coste, Bastien Joubert, Virginie Desestret, Roland S Liblau, Jérôme Honnorat

Original Article

A pilot study to develop Paraneoplastic Cerebellar Degeneration mouse model

Fabrice Faure,[1] Lidia Yshii,[2,3,4,5] Toufic Renno,[6] Isabelle coste,[6] Bastien Joubert,[1,7] Virginie Desestret,[1,7] Roland Liblau,[2,3] and Jérôme Honnorat[1,7]

[1] Synaptopathies and Autoantibodies (SynatAc) Team, Institut NeuroMyoGène (INMG)-MeLis, INSERM U1314, CNRS UMR 5284, Université de Lyon, Université Claude Bernard Lyon 1, 69373 Lyon, France

[2] Toulouse Institute for Infectious and Inflammatory Diseases (Infinity), University of Toulouse, CNRS, INSERM, UPS, 31024 Toulouse, France

[3] Department of Immunology, Toulouse University Hospital, 31300 Toulouse, France

[4] KU Leuven, Department of Microbiology, Immunology and Transplantation, and [5] Department of Neurosciences, Leuven 3000, Belgium

[6] Cancer Research Centre of Lyon, Université de Lyon, INSERM 1052, CNRS 5286, 69008 Lyon, France

[7] French Reference Centre on Paraneoplastic Neurological Syndromes and Autoimmune Encephalitis, Hospices Civils de Lyon, Hôpital Neurologique, 69677 Bron Cedex, France

Contributions:

Fabrice Faure: acquisition, analysis and interpretation of the data, drafting the manuscript for intellectual content and figures.

All authors : critical revision of the manuscript for important intellectual content

Pr Roland Liblau, Pr Jérôme Honnorat: study concept and design, analysis and interpretation, critical revision of the manuscript for important intellectual content, study supervision.

Corresponding author: Professeur Jérôme Honnorat, Neuro-Oncologie, Hôpital Neurologique Pierre Wertheimer, 59 Boulevard Pinel, 69677 Bron Cedex, France ; jerome.honnorat@chu-lyon.fr ; Phone : +33 4 72 35 78 08 ; Fax : +33 4 72 35 73 29.

ABSTRACT

Objective:

Modeling Paraneoplastic Neurological Diseases to understand the immune mechanisms leading to neuronal death is a major challenge given the rarity and terminal access of patients' autopsies. Here, we present a pilot study aiming at modeling Paraneoplastic Cerebellar Degeneration with Yo-autoantibodies (Yo-PCD).

Methods:

Female mice were implanted with an ovarian carcinoma cell line expressing CDR2 and CDR2L, the known antigens recognized by anti-Yo antibodies. To boost the immune response, we also immunized the mice by injecting antigens with diverse adjuvants and Immune Checkpoint Inhibitors. Ataxia and gait instability were assessed in treated mice as well as autoantibody levels, Purkinje cells density, and immune infiltration in the cerebellum.

Results:

We observed the production of anti-Yo antibodies in the CSF and serum of all immunized mice. Brain immunoreaction varied depending on the site of implantation of the tumor, with subcutaneous administration leading to a massive infiltration of immune cells in the meningeal spaces, choroid plexus, and cerebellar parenchyma. However, we did not observe massive Purkinje cells death nor any motor impairments in any of the experimental groups.

Interpretation:

Self-sustained neuro-inflammation might require a longer time to build up in our model. Unusual tumor antigen presentation and/or intrinsic, species-specific factors required for pro-inflammatory engagement in the brain may also constitute strong limitations to achieve massive recruitment of antigen-specific T-cells and killing of antigen-expressing neurons in this mouse model.

KEYWORDS

Paraneoplastic Cerebellar Degeneration, Autoantibodies, anti-Yo autoantibodies, CDR2L protein, Immune Checkpoint Inhibitors

INTRODUCTION

An animal model of paraneoplastic cerebellar degeneration (PCD) would be useful to decipher the immune mechanisms leading to the neurological damages observed in this disease, particularly those associated with anti-Yo antibodies (Yo-PCD), which are the most frequent[1]. In patients, it is near to impossible to analyze the pathological mechanisms leading to Purkinje cells death because of the lack of cerebellum pathology at the early stage of the disease. Moreover, only few post-mortem analyses are available; they are performed late after the onset of the immune process when most, if not all, Purkinje cells have been eliminated[2,3].

Attempts to transpose this pathology to an animal model remains unsatisfactory. Initial studies were unsuccessful in triggering Purkinje cell loss by infusion of IgGs or lymphocytes from Yo-PCD patients into brains of wild-type or severe combined immunodeficiency (SCID) mice[4]. Active immunization in a variety of mouse strains[5–7] against cerebellar degeneration-related protein 2 (CDR2), the only suspected Yo-antigen at that time, resulted in humoral and cell-mediated immune responses, albeit not accompanied by any pathological change.

Taken together, these datas highlight the inability of Yo auto-antibodies alone to interfere in vivo with Purkinje cell integrity, and the difficulty for peripherally-activated lymphocytes to translocate into brain parenchyma in such experimental settings. In support of the central role of T-lympthocytes in PCD immunopathology, a more recent model of PCD, based on transgenic mice expressing haemagglutinin (HA) as a *neo*-self Purkinje cell antigen and implantation of HA-expressing tumor cell line, was shown to depend on CD4+ and CD8+ T-cells activation against HA[8]. Importantly, for these transgenic mice to develop ataxic symptoms, adoptive transfer of heterologous HA-specific T-cells had to be co-injected with an anti-CTLA-4 immune checkpoint inhibitor (ICI)[9]; only then were they able to infiltrate the brain and lyse HA-expressing Purkinje cells. However, this model does not target the antigens involved in human Yo-PCD, and other models closer to pathophysiological conditions are necessary. Recent work demonstrated that CDR2, long thought to be the principal antigen in Yo-PCD, is not the only autoantigen involved, and that CDR2 Like (CDR2L), which has 45% sequence identity to CDR2[10], might be in fact the major antigenic target[11,12]. In addition, proinflammatory tumor microenvironment could also play a role in breaking immunotolerance through T-cell activation[13–15], since Yo-PCD tumors are highly infiltrated by immune cells compared to non-PCD tumors; they also harbor specific mutations of CDR2 and/or CDR2L genes and overexpress CDR2L[16]. These are strong arguments in favor of both CDR2 and CDR2L as model neo-antigens to target in a Yo-PCD mouse model. In this study, we therefore aimed at inducing a strong immune response in mice with syngenic ovarian cancer expressing both CDR2 and CDR2L, which has never been done to our knowledge,

to develop a functional model of Yo-PCD with a paraneoplastic component related to the underlying gynecological cancers as observed in women with Yo-PCD.

EXPERIMENTAL PROCEDURES

MICE

C57Bl/6J female mice were obtained from Janvier Labs (Le Genest-Saint-Isle, France) and kept in UAR3453-US7 conventional animal facility, Lyon, France. All experiments were performed in accordance with the European Union guidelines and approval by local ethics committee (#6316-2016080410268068 and #24283-2019090614526169, Comité d'éthique en expérimentation animale de l'Université Lyon 1 CEEA- UCBL 55).

CELL LINE

HEK-293 (#CRL-1573, ATCC, VA, USA) cells were cultured in GlutaMax High glucose Dulbecco's Modified Eagle Medium (#10569010, Fisher Scientific Gibco, Illkirch, France) supplemented with sodium pyruvate, 10% fetal bovine serum and penicillin/streptomycin (37°C, 5% CO2).

ID8 Mouse Ovarian Surface Epithelial (MOSE) cells (kind gift from T.Renno, CRCL Lyon) were used to develop a syngeneic mouse model with growing ovarian cancer as previously described[17]. Cells were cultured as HEK-293 but with 5% fetal bovine serum.

IMMUNOFLUORESCENCE STAINING OF ID8 CELLS AND AUTO-ANTIBODIES DETECTION BY HEK-293 CELL-BASED ASSAY

ID8 cells were grown in a 24-well plate on 14mm round cover glasses coated with poly-L-Lysine wt 150,000-300,000 ((#P1399, Sigma-Aldrich, Lyon, France), as were HEK-293 cells for detection of auto-antibodies in serums; whereas for detection in CSF, HEK-293 were grown in poly-L-Lysine-coated IbiTreat Angiogenesis 96 Well µ-Plate (#89646, Ibidi, Gräfelfing, Germany).

For detection of auto-antibodies, HEK-293 cells were transfected with GFP-tagged Mouse CDR2 plasmid (#MG51762-ACG, Sino Biological, Eschborn, Germany) and GFP-tagged Mouse CDR2L plasmid (cloning strategy below) using Lipofectamine LTX with Plus reagent (#15338100, Fisher Scientific Invitrogen). Briefly, GFP was amplified from peGFP-N3 vector (Clontech, Mountain View, CA) to replace C-term 6His-tag in

pCDNA3.1(+)-mCDR2L (# OMu01475C, Genscript, Leiden, Netherlands) using CloneAmp™HiFi PCR (#639298, Clontech) and In-Fusion HD Cloning Plus kit (#638920, Clontech). The following incubation steps were performed 24h after transfection at room temperature and protected from light. Cells were washed in phosphate-buffered saline (PBS) before and after 15 min fixation with 4% PFA in PBS, followed by blocking and permeabilizing with 0.2% gelatin, 0.1% Triton in PBS for 90 minutes. Cells were then incubated with diluted serum (1/20) or diluted CSF (1/10) in buffer for 90 minutes. After washing in PBS, cells were finally incubated for 1 hr with 2µg/mL Alexa Fluor 647 Goat anti-IgG (H+L) Highly Cross-Adsorbed species-specific secondary antibody (#A-21236 and A21445, Fisher Scientific Invitrogen) and 0.25µg/mL DAPI (Sigma-Aldrich**).**

For IF staining, ID8 cells were fixed, blocked and permeabilized as mentioned above. Cells were then incubated 1½ hr at room temperature with 1:40 anti-CDR2 (#54845, Abcam, Paris, France) or 1:50 anti-CDR2L antibody (#HPA022015, Sigma-Aldrich), or a 1:20 diluted cerebrospinal fluid (CSF) from Yo-positive patient as a positive control. After washing in PBS, cells were finally incubated for 1 hr with 2µg/mL Alexa Fluor 488 goat anti-IgG (H+L) Cross-Adsorbed species-specific secondary antibodies (#A11034, # A11029, and #A11013, Invitrogen, Carlsbad, CA) and 0.25µg/mL DAPI (Sigma-Aldrich) protected from light.

ID8 cells and HEK-293 cells processed in 24-well plates were washed in PBS before transfer of round cover glasses with attached cells onto glass microscope slides (#LR45D, Fisher Scientific Menzel) and mounted using FluorSave Reagent (#345789, Sigma-Aldrich Calbiochem). Slides were imaged under Zeiss Axio imager Z1 Microscope, whereas HEK-293 cells in 96-wells µplaque were imaged under Zeiss Axiovert 200M inverted Microscope**.** Images were further processed with ImageJ public domain software (Wayne Rasband, NIH).

FACS ANALYSIS

PD-L1 cell surface expression was assessed in basal condition and after 36h incubation of ID8 cells with 75ng/mL mouse interferon-γ (#485-MI, Bio-Techne, Rennes, France). Cells were then detached with trypsin 0.25%, washed twice and incubated 10min with anti-mouse CD16/CD32 (#101319, Biolegend, San Diego, USA) for blocking non-specific binding of immunoglobulin to the Fc receptors. Then, cells were stained for 30 min at 4°C with Phycoerythrin (PE)-labelled anti-mouse CD274 antibody (10F.9G2, Biolegend) [1:100, v/v] or PE-labelled mouse IgG isotype control antibody (RTK4530, Biolegend), and washed with FACS buffer. Data was acquired on a Canto II flow cytometer (BD Bioscience, NJ, USA) and the percentage of PD-L1 expressing cells was determined using FLowJo 1.52p software (Wayne Rasband NIH, USA, public domain).

RECOMBINANT PROTEINS

Mouse CDR2 and CDR2L cDNAs were cloned, respectively from the pCMV3/mCDR2 (#MG51762-CH, Sino biological) and pCDNA3.1(+)/mCDR2L (# OMu01475C, Genscript) plasmids, into a pET-28b vector backbone containing a C-Term His tag (#69258, Sigma-Aldrich Novagen), using the CloneAmp™HiFi PCR (#639298, Clontech) and In-Fusion HD Cloning Plus (#638920, Clontech) kits.

BL21 (DE3) and BL21 (DE3) Codon Plus bacteria (#230192 and #230240, Agilent, Les Ulis, France) were used to amplify CDR2 and CDR2L recombinant proteins, respectively. The transformed BL21 were grown in lysogeny broth containing 30 µg/mL Kanamycin for standard BL21, plus 50µg/mL Chloramphenicol and 75µg/mL Streptomycin for BL21 Codon plus strain. Protein expression was induced by incubation for 2 hrs with 1.0 mmol isopropyl β-d-thiogalactoside (IPTG). Inclusion bodies were obtained after 15 min incubation at 30°C with lysozyme (Sigma-Aldrich) followed by sonication on ice and centrifugation. Pellets were solubilized in Denaturing solubilization Buffer LEW from Macherey Nagel's kit mentioned hereafter containing 8M Urea for 60min on a rotating agitator at 4°C.

Supernatant was applied to a pre-equilibrated Protino Ni-IDA column (#745160, Macherey Nagel, Hoerdt, France) at room temperature for binding. Recombinant proteins were purified by gravity flow in Denaturing Elution buffer containing 250mM imidazole. Finally, eluate was concentrated and buffer exchanged on vivaspin-6 columns 10kDa MWCO (#VS0601, Sartorius, Goettingen, Germany) to a final concentration of urea and imidazole reduced to 4M and 4mM, respectively. Concentration of recombinant proteins was determined with Micro BCA Protein assay kit (#23235, Fisher Scientific). Purity and identity of proteins were evaluated by SDS-PAGE on 4-12% polyacrylamide XT Bis-Tris gels (#3450123, Bio-Rad, Marnes-la-coquette, France) followed by Coomassie staining (#17524, Serva, Heidelberg, Germany), and by western blot analysis with anti-His (#MA1-21315, Fisher Scientific), anti-CDR2 (#Ab 54845, Abcam) or anti-CDR2L primary antibody (#HPA022015, Sigma-Aldrich) followed by species-specific HRP-conjugated anti-IgG secondary antibody (#111-036-003 and #115-036-003, Jackson Immunoresearch, Cambridgeshire, UK) and Substrat HRP Immobilon Western (#WBKLS0500, Sigma-Aldrich Millipore) revelation kit. Chemiluminescence signal was acquired on a Chemidoc imaging system (Bio-rad).

WHOLE TUMOR ANTIGENS PREPARATION

Necrotic cell preparation

ID8 cells were grown until reaching 80% confluency. One flask was incubated for 1hr at 42°C and then for 2 hrs at 37°C, while another flask was incubated for 1hr at 37°C in normal medium containing 0.06% Squaric acid

(#123447, Sigma-Aldrich) in order to improve the immunogenicity of tumor cell antigens. Cells were then detached, washed twice in PBS and mixed in a 1:1 ratio to a final 4.10^7 cells/mL in PBS. Cells were further subjected to 6 freeze and thaw cycles consisting of 3 minutes incubation in liquid nitrogen followed by 3 minutes at 42 °C. Cells were then sonicated on ice (3 cycles of 30sec at 20W). Complete necrosis was confirmed by trypan blue staining and protein concentration was determined with Micro BCA Protein assay kit (#23235, Fisher Scientific). Lysates were aliquoted and stored at -80°C.

Gamma-irradiated cell preparation

ID8 cells grown until reaching 80% confluency were irradiated in sealed flasks using an X-RAD 320 irradiator (Precision X-Ray, CT, USA) for 60 min at 2.47Gy/min (320kw, 12.5mA, 150 Gy). Cell viability was assessed by Trypan blue dye exclusion. Cells were then resuspended at 4.10^7 cells/mL in PBS and used immediately in the immunization mix. Apoptosis was assessed using a *FITC Annexin V Apoptosis Detection Kit with PI* (#640914, Biolegend) and a Canto II flow cytometer on a small aliquot. Data were analyzed with FLowJo 1.52p software.

TUMOR INOCULATION, VACCINATION PROTOCOLS AND TREATMENTS

Subconfluent ID8 cells were detached in trypsin 0.25%, washed twice, and a single-cell suspension prepared in PBS or PBS mixed with an equal volume of 12mg/mL cold Matrigel (#E1270, Sigma-Aldrich). For intraperitoneal implantation, 5.10^6 ID8 cells in a volume of 200µL were injected in the peritoneal cavity of 8-week-old C57Bl/6 mice. End point was monitored by measuring abdominal perimeter every other day to follow ascites development. Tumor growth was assessed by measuring tumor burden on peritoneum and diaphragm at end-point. For subcutaneous implantation, 7.10^6 ID8 cells in a volume of 100µL were injected s.c into the right flank of mice. Tumor growth was measured every other day using a digital Vernier calliper. Tumor volume is expressed in mm^3 and calculated as $V= 0.52 \times D \times (d)^2$, where D is the longest diameter and d the perpendicular one. Subcutaneous tumors did not display ulceration nor reached $2500mm^3$ end-point volume (17mm D diameter).

The following experimental designs (see figure 1) were setup.

Design A

Following IP tumor cell line implantation at day 0, immunization started at day 30; 75µg of CDR2 and 75µg of CDR2L recombinant proteins were mixed with 50µg poly(I:C) (#vac-pic, Invivogen, Toulouse, France) in PBS and injected s.c in the lower back. One booster injection was made on day 42 with half the quantity of proteins. IP

injections of 200µg inVivoMAb anti-mouse PD-1 (#BE0146, BioXcell, NH, USA) were done once every other day from day 38 to 46. Mice reached end-point on week 11.

Design B

Following IP tumor cell line implantation at day 0, immunization started at day 7 with booster injections at day 18 and day 42. Immunization and bosster mixes were similar to those of *design A*. Different ICI treatments were applied to seperate groups of mice: 200µg inVivoMAb anti-mouse PD-1 (#BE0146, BioXcell) were injected IP, along with 100µg anti-CTLA-4 (gift from R. Liblau) or 200µg inVivoMAb anti-mouse LAG-3 (#BE0174, BioXcell). ICIs were delivered a few hours before booster injection on day 18 and 42, and the day before; then injections were made twice a week from week 4 to 7, then once a week from week 8 to 13. Mice reached end-point on week 13.

Design C

Immunization protocol started at day 0, followed by IP tumor cell line implantation at day 14. Immunization mix was prepared with 75µg of each CDR recombinant proteins and 100µg necrotic whole tumor antigens emulsified as described[18] with Complete Freund's adjuvant (CFA) containing 1mg/mL heat-killed *Mycobacterium tuberculosis* (#vac-cfa, Invivogen) at a 1:1 ratio. Each mouse was injected s.c with 200µl emulsion in its lower back. Booster s.c injections were performed on day 13 and 35 with half dose of proteins and tumor antigens in PBS supplemented with 50µg poly(I:C). A few hours before injections at immunization day 0 and booster day 13, 50µg of agonistic InVivoMAb anti-mouse CD40 (#BE0016-2, BioXcell) were injected IP. 400ng Toxine Pertussis (#3097, Bio-Techne) was injected IP on booster days (d13 and 35), and 200ng two days later. In addition, 200µg anti-PD-1 plus 100µg anti-CTLA-4 ICI treatment was delivered a few hours before booster injection on day 13 and 35 and the day before on day 12 and 34, then injections were made twice a week until week 14. Mice reached end-point on week 14.

Design D

Immunization protocol started at day 0, followed by s.c. tumor cell line implantation at day 14. 50µg poly(I:C) adjuvant was added to every s.c antigenic injection and 50µg anti-CD40 was injected IP a few hours before. First injection contained CDR proteins and whole tumor antigens emulsified in CFA as described[18] but with whole tumor antigens prepared as a 1:1 mix ratio of necrotic and irradiated apoptotic ID8 cells. Subsequent booster injections on day 13 and day 35 were performed with half dose of proteins and tumor antigens in PBS. 400ng

Toxine Pertussis was injected IP on booster days (d13 and 35), and 200ng two days later. ICI treatment was identical to that of design C. Finally, to strengthen anti-tumoral immune response, every other day injections of histone deacetylase inhibitor (HDACi) Entinostat (#6208, Bio-Techne Tocris) or DNA methyltransferase inhibitor (DNMTi) 5-Azacitydine (#3842, Bio-Techne Tocris) were done alternatively for 3 weeks starting on day 18. Experiment was ended week 13 for analysis.

MOTRICITY AND BALANCE ANALYSIS

Recording of tests started after first immunization challenge and was carried out every week until the end of the experiment.

To assess motor coordination, mice were subjected to rotarod tests on a Panlab rotarod (#LE8205, Biosed, Vitrolles, France). The procedure consisted in measuring the time the mouse can remain on a rotating rod before falling. Mice were first habituated to walk on the rod at 14rpm speed, then trained over 3 consecutive days on an accelerating rotarod (from 14 to 44rpm over 210 seconds - 1rpm increase every 7 seconds) performing 2 trials a day with 20min rest between trials. Tests were then recorded weekly on the same day with a 20 min rest between trials. First test was performed on the accelerating rotarod at increasing speed as mentioned previously, with the best value of 2 trials kept for analysis. Second test was performed on a single trial with the rotarod constantly running at 22rpm for at most 120 seconds.

To assess the balance and gait stability of mice, we measured the time needed for mice to walk along beams of 13mm or 6mm width, on a distance of 80cm. Mice were first habituated to walk along the beam towards a nesting box without stopping or freezing. Then, they were trained for 3 days to cross each beam twice with 20min rest between beam changes. Recordings were made once a week with the best value of 2 trials per beam kept for analysis.

TISSUE PROCESSING AND IMMUNOHISTOCHEMISTRY

CSF was punctured from the cisterna magna as described previously[19] on anesthetized animals. Blood, ascites, tumor tissues and brain were collected right after decapitation. Blood and ascites were set to clot for 15-30 minutes at room temperature and centrifuged at 1500g for 10 minutes to collect serum as the upper phase. Serum was kept in dry ice before storage at -80°C. Tumor tissues and sagittal half-cut brains were fixed overnight in formalin quickly after removal. After transfer in PBS, samples were processed for paraffin impregnation and embedding. Briefly, in a cassette the sample is dehydrated in baths of increasing concentrations of ethanol (70-85-90%-

absolute), then ethanol is cleared in 3 successive 100% butanol baths before impregnation in warm paraffin and embedding into a paraffin mold. Paraffin-embedded samples were frozen at -20°C the day before to be cut, and 5µm sagittal slices were made on a LEICA RM2245 microtome (Leica Microsystems, Nanterre, France) and laid on superfrost slides (#J1800AMNZ, Labelians, Nemours, France). Slices were dried at 45°C for 1hr and left overnight at room temperature before storage. Alternatively, some tumor tissues and rat brains were fixed quickly after removal in 4% paraformaldehyde for 6 hrs at 4°C, then rinsed for 1h in 0.1M Phosphate buffer pH 7.4 at 4°C, and dehydrated overnight in 30% sucrose at 4°C. Biopsies were then frozen in OCT medium and stored at -20°C. 10µm slices were cut on a cryostat apparatus and laid on superfrost slides. Slides were stored at -20°C.

Histological Hematoxylin Eosin (H&E) stainings were made on fixed sample slices either paraffin-embedded or frozen. Briefly, before staining and where applicable, paraffin was removed in 3 successive methylcyclohexane baths then sample slices were rehydrated in baths of decreasing concentrations of ethanol (Absolute - 95% - 70%). After total rehydration in tap water of frozen or dewaxed sample slices, staining was done with 5 min rinsing steps in tap water between each incubation. Starting in Mayer's hematoxylin (#05-M06002, Eurobio Scientific, Les Ulis, France) for 5 min then differentiated in 1% Hydrochloric acid in ethanol for 15 seconds, and in Eosin-Phloxine (#05-M10020, Eurobio Scientific) for 30 seconds. Dehydration was made in baths of increasing concentrations of ethanol (70% - 95% - Absolute), then clearing made in 3 successive methylcyclohexane baths before mounting a glass coverslip with Pertex (#00811, MM France, Brignais, France) on the slide.

For immunostaining, 5µm sections of formalin-fixed paraffin-embedded (FFPE) brain slices were deparaffinized and rehydrated before heat mediated epitope retrieval (citrate buffer, pH 6.0). Then, FFPE sections and 10µm fixed frozen sections were processed similarly as follows. Inactivation of endogenous peroxidases was performed by incubation with PBS/1% H_20_2 for 15 min. Sections were permeabilized and blocked for unspecific binding for 1hr at room temperature in 0.3% Triton-1% BSA-1% normal goat serum in PBS, and incubated overnight at 4°C with a single antibody at the following dilution (v/v): 1:1000 monoclonal mouse anti-Calbindin-D-28K antibody (#CB-955, Sigma-Aldrich), or 1:500 polyclonal Rabbit anti-GFAP Ab (#Z0334, Agilent), or 1:200 polyclonal Rabbit anti-Iba1 Ab (#019-19741, Fujifilms Wako Chemicals, Neuss, Germany), 1:150 Polyclonal Rabbit Anti-CD3 Ab (#A0452, Agilent), or 1:100 monoclonal rat anti-CD8a Ab (#14-0808, Fisher Scientific eBiosciences), or 1:800 Monoclonal Rat anti-Mouse MHC Class I H-2b (#MCA2398, Bio-rad) or 1:100 serum from mice. Sections were then incubated for 45 minutes with 1:1000 species-specific Biotin SP-AffiniPure Goat anti-IgG Fcγ fragment specific secondary antibody (#115-065-008; #111-065-008, #112-065-071, or #109-065-008 Jackson ImmunoResearch). Antibody binding was amplified with Vectastain Elite ABC-HRP kit (#PK6100, Vectorlabs,

CA, USA) before peroxidase activity was revealed with Diaminobenzidine substrate (#K3467, Agilent) and nuclei counterstained with Mayer's hematoxylin (#05-M06002, Eurobio Scientific). Dehydration, clearing and mounting was made as detailed above in H&E stainings. All images were acquired on a Zeiss Axio scan Z1 using a 3CCD Hitachi HV-F303SCL Camera in the bright field setting at 20x magnification. Images were analysed with Zeiss ZEN 2.5 lite software.

Purkinje cells were counted in vermis region (0.72mm) and hemisphere region (2.64 mm from the midline) on three serial sagittal slices per region. Icy Spot detector (2.4.1.0 BioImage analysis software, Pasteur) was used to count Purkinje cells and measure the length of Purkinje cell layer to calculate density as cell/mm.

STATISTICAL ANALYSIS

Statistical analysis was performed using GraphPad Prism 7.0 software. Comparisons between multiple groups were performed using the non-parametric Kruskal Wallis test with Dunn's post-hoc test. For comparison of tumor growth curves and behavioral analysis, we used repeated measures 2-way ANOVAs (Sidak or Dunnet's post-test) to assess the variation of data over days. Results were considered significant when p-value was <0.05. The levels of significance were indicated as follow: *$p < 0.05$, **$p < 0.01$, and *** $p < 0.001$. Group sizes and statistical tests performed are indicated in the corresponding figure legends.

RESULTS

OVARIAN CANCER MODELING

ID8 MOSE (Mouse Ovarian Surface Epithelial) cells were used to develop a syngeneic ovarian cancer[17] in C57Bl/6 mice. These tumor cells express CDR2 and CRD2L (**figure 2A**). Expression of PD-L1 by the ID8 cells is strongly induced in vitro upon interferon-gamma (IFN-γ) stimulation (**figure 2B**), suggesting that ID8 cells could have the capacity to inhibit T-cell responses in inflammatory conditions through the binding of T-cell's PD-1 receptors. Hence a possible requirement for the use of ICI anti-PD-1 in our model. Female mice were first implanted intraperitoneally (IP) and tumor progression was assessed at end-point (**figure 2C**), usually 12 weeks after implantation when ascites fluid developed.

FIRST MODEL: IMMUNIZATION AGAINST BOTH CDR2 AND CDR2L

To direct the anti-tumor immunity towards both CDR2 and CRD2L onconeural antigens, we performed an active immunization with CDR2 and CDR2L recombinant proteins mixed with poly(I:C) as an adjuvant used to stimulate CD4 and CD8 T-cell anti-tumor immunity[20,21]. Subcutaneous injections were made on day 30, 4 weeks after ID8 cells IP implantation, then on day 42 for a single challenge (**figure 1A**). ICI (anti-PD-1) treatments were injected 5 times every other day starting 4 days before challenge. The end-point was reached at week 11. ICI-treated immunized mice (n=6) were analyzed along with control mice only implanted with the tumor (n=6) and littermate controls (n=6). In this first model, auto-antibodies against CDR2 and CDR2L were detected in the serum and CSF of tumor-bearing, immunized mice but not in non-immunized control mice implanted with the tumor (**figure 3A and B**). However, no alteration of motricity or balance, nor inflammatory infiltrates in the brain or loss of Purkinje cells was observed in immunized mice (data not shown), and tumor burden was not decreased compared to non-immunized animals.

IMPROVEMENT OF ANTI-TUMORAL IMMUNE RESPONSE

As we did not observe an efficient anti-tumoral immunity in our first experimental protocol, we sought to strengthen it using different strategies (**figure 1B and 1C**):

- Immunization was started earlier, close to the ID8 cells implantation to anticipate tumor progression and we also performed a second challenge on day 35.
- In the event that unknown antigens could be necessary to trigger an efficient anti-tumor immune reaction, an ID8 cell necrotic lysate[22] was added to CDR2 and CDR2L proteins in the immunization mix.
- poly(I:C) was first used as a single adjuvant then changed in order to trigger a stronger Th1-type immune response. Complete Freund's Adjuvant (CFA)[23] emulsion of antigens was used as the initial injection. Then, both challenges were done using poly(I:C) associated first with anti-CD40 agonist to activate dendritic cells and enhance T-cell priming with tumor antigens[24,25], and second with Pertussis Toxin (PTX)[26–28], known to modify the permeability of Blood Brain Barrier (BBB) and promote entry of T-cells to the CNS in the presence of IFN-γ [29].
- Finally, we used anti-CTLA-4 or anti-LAG-3 combined with anti-PD-1[30,31] delivered twice a week during 10-11 weeks (until end-point) starting on the day before challenge to stimulate T lymphocytes reaction.

Each group (n=6) was comprised of immunized mice differing according to adjuvants used and ICI molecules injected (**figure 1B and 1C**).

As in the first experimental protocol, we observed production of anti-CDR2 and anti-CDR2L auto-antibodies in the sera and CSF of immunized mice, but there was neither evidence of tumor regression at end-point nor any clinical signs of ataxia through behavioral tests. Purkinje cell density and morphology were normal, and no specific phenotype or distribution of microglial and astrocytic glial cells, nor any infiltrating T or B lymphocytes were observed in the brain parenchyma (data not shown). The use of ICIs to dampen the PD-L1-induced inhibition of T cells in the tumor was also ineffective, suggesting that other mechanisms in the tumor environment are capable of blocking activation of immune cells in the peritoneum. This led us to question the immunogenicity of the tumor cell line following IP implantation[32].

MODIFICATION OF THE TUMOR IMPLANTATION SITE

In an attempt to increase the immunogenicity of the tumor, we inoculated ID8 cells s.c. instead of IP one day after d13 immunization challenge and maintained treatment with anti-PD1 and anti-CTLA-4 antibodies (**figure 1D**). Immunization cocktail was enriched extemporaneously with γ-irradiated ID8 cells showing 10% late stage apoptosis on the day of irradiation[33,34] in addition to the necrotic lysate and recombinant CDR proteins previously used. Each antigenic load was associated to poly(I:C) and anti-CD40 agonist combination[25], first with CFA, then on both challenges with PTX[25–27]. We also tried to reduce immunosuppression by treating mice with histone deacetylase inhibitor (HDACi) Entinostat[35] and DNA methyltransferase inhibitor (DNMTi) 5-Azacitydine[36–38] starting 4 days after s.c implantation of tumor. These 2 epigenetic modifiers were shown to synergize with anti-PD-1 through type-I IFN signaling and induce MHC-class II expression in tumor cells, impeding tumor growth[35–38]. The protocol was stopped 10 weeks after both ID8 cell implantation and d13 challenge. Groups composed of immunized mice (n=6), control mice only implanted with the tumor (n=6) and littermate controls (n=6) were analyzed.

ID8 cells subcutaneous growth was minimal and declined similarly in both immunized and non-immunized animals (**figure 4A**). Post-mortem analysis showed an important splenomegaly in tumor-bearing mice, immunized or not, compared to littermate controls, and especially in the non-immunized ones (n=6, $p<0.0001$) (**figure 4B**); showing the praramount role of the subcutaneous implantation of tumor cells in our model to trigger a strong immune response. As with the previous protocols, CSF and serum from immunized animals contained auto-antibodies against CDR2 and CDR2L, and we confirmed that these serums reacted with Purkinje cells (**figure 3C**). However, in contrast with the previous protocols a reduction of Purkinje cells density in the cerebellar hemisphere (n=6, p=0.0256) was observed, but not in the vermis, of immunized animals, compared to non-immmunized

animals (**figure 4C**). Nevertheless, motricity performance and balance of mice was not impaired during the protocol (data not shown). Furthermore, both immunized and non-immunized tumor-bearing mice displayed a massive brain infiltrate of CD3+ and CD8+ lymphocytes in meninges, perivascular zones, choroid plexus and the cerebellar parenchyma (**figure 4D and 4E**). However, no CD19+ B lymphocytes were observed (data not shown). Of note, in one mouse from each group, infiltrating CD8+ lymphocytes were observed in contact with some Purkinje cells **(figure 4D)**, suggesting a possible immune reaction targeting Purkinje cells. Whereas subcutaneous rather than IP implantation of ID8 cells has shown a clear benefit to initiate infiltration of T cells in the brain (**figure 4E**), with greater numbers that infiltrated the cerebellar parenchyma of immunized mice (**figure 4F**), we observed limited damage in the cerebellum. Compared to littermate controls, tumor-bearing animals showed an enhanced expression of MHC Class-I in the choroid plexus epithelium, ependymal cells, and endothelium at meningeal perivascular sites (**figure 4G**), which seems to match with the sites showing T cell infiltration. By contrast, Purkinje cells showed no detectable expression of MHC Class-I molecules (**figure 4G**).

DISCUSSION

In the present pilot study, we attempted to develop a Yo-PCD mouse model summarizing the main characteristics of patients[2,39,40] that are: (i) anti-CDR2 and CDR2L auto-antibodies found in serum and CSF, (ii) expression of CDR2 and CDR2L in the underlying tumor, (iii) Purkinje cells loss, and (iv) cerebellar clinical signs. We combined ICI treatment and tumor cell line implantation with active immunization against CDR2 and CDR2L coupled to diverse adjuvants such as CFA, PTX and poly(I:C). Although we were able to stimulate autoantibodies production and diffusion in the CSF, as well as a mild immune reaction in the cerebellum and a weak Purkinje cells loss, we were unable to provoke cerebellar ataxia.

In our IP tumor-implanted models, the anti-tumor immune response was unable to reduce tumor burden hence the absence of any inflammatory cells in the brain or Purkinje cell loss. Conversely, the s.c implantation of our tumor cell line induced a strong immune response that was able to reduce tumor burden very quickly without the need of immunization. Interestingly, this led to T cell migration to the brain including cerebellar parenchyma and an increase of spleen weight suggesting a massive peripheral immune reaction. The specificity of this infiltrate remains elusive as we were able to only see a few CD8+ T-cells in contact with Purkinje cells in two animals, surprisingly including a non-immunized mouse. Thus, whole cerebellum analysis would be required to assess the extent of this observation in other animals and to demonstrate a broad Purkinje cell loss since we analyzed two

restricted zones of which only the cerebellar hemisphere of immunized mice showed a slight reduction in Purkinje cell density, unlike non-immunized mice. Although active immunization in tumor-bearing animals did not prove beneficial as to the density of the total infiltrate compared to non-immunized mice, it is meant to favor T cell specificity. A possible explanation for this quantitative discrepancy might be the dual role of Pertussis Toxin (PTX) adjuvant. It was used here for its ability to enhance pathogenic autoimmunity[27], but PTX is also a known chemotaxis inhibitor[41] and could potentially compromise migration of antigen-specific T-cells into brain parenchyma[42,43] despite altering BBB integrity. Additional treatment with pro-inflammatory molecules should be able to overcome this potential inhibition. Importantly, as mentioned in a clinical study, the observation of infiltrated T lymphocytes seems to be confined to early pathogenesis[2], and not observed later once irreversible neuronal injury has occurred. Therefore, more time may be required to see extensive damage of Purkinje cells in our s.c Yo-PCD model.

As demonstrated in previous Yo-PCD animal models[5,44] using CDR2 as target antigen, Yo-Abs are not able to induce Purkinje cells loss on their own, which we confirmed with immunization against both CDR2 and CDR2L. Hence the major hypothesis of a T-cell-driven pathomechanism in Yo-PCD[3,15,45] with T-cell priming in the underlying tumor. A review of the different attempts to model PNS in animals (**table 1**) highlights the difficulty to induce autoimmunity with endogenously activated T-cells specific for an intracellular neuroantigen. After the initial unsuccessful trials in which patient IgGs or mononuclear cells were injected into mouse brains[5], the use of non-autologous antigens for immunization in early models[4,6,7,46] was a strong limitation, as was the absence of implanted tumor cell line[47], or if any, its non-syngeneic origin[46]. Although the use of an endogenous self-antigen immunization was reported in a rat model (table1: PNMA1) combined with adoptive transfer of antigen-specific CD4+ T-cells[47], it has proven unsuccessful without an underlying tumor. We therefore propose that a syngeneic tumor model could be a possible basis for PCD pathogenesis modeling. since tumor-specific immune response could be involved in the tolerance breakdown against onconeural antigens and subsequent auto-immunity observed in Yo-PCD. We may question the penetration of pathogenic mechanisms due to genetic differences of animal species or mouse strains. Beyond the pathogenic effect of Yo antibodies observed in vitro in rat organotypic slice cultures with CSF or serum from patients[48,49], the in vivo experiments made in rat[50] or guinea pig[51] did not translate into neuronal damage or ataxia. In a similar way, as reviewed in Table 1 of our article, early models were tested in various mouse strains but none have preferentially succeeded to produce disease. In the context of our model of Yo-PCD where we try to recapitulate pathomechanisms from the induction phase (tolerance breakdown) to the effector phase (CNS damage), we think that a mouse model is a better choice for different reasons. First of all, as

we eventually aim at exploring specific mechanisms and therapeutic targets, we will ultimately need to choose from a large number of transgenic and KO animals that are likely available in mouse rather than rat, and even more on a B6 background. These will be an essential extension of the Yo-PCD model. Secondly, the B6 mouse strain is clearly identified as a Pro-Th1 immunity model as opposed to the BalB/c that is considered a pro-Th2 model[52]. This is why we favor the B6 model that suits our hypothesis of a cellular immune-mediated mechanism, while not ruling out a possible amplification of the disease induced by auto-antibodies. Lastly, we can also benefit from a more exhaustive literature in modeling pathogenic immune mechanisms in mouse.

In our model of Yo-PCD, we seek for a strong amplification of a highly specific adaptive immune response against CDR2 and CDR2L with the advantage of manipulating endogenous immune mechanisms that can reflect the physiopathology of patients. Recently, more artificial transgenic models using unconventional-self antigens (table1: HA[8], β-Gal[53]) expressed in both tumor and brain succeeded in inducing neuronal damage. These models used adoptive transfer of large numbers of specific TCR-transgenic T-cells in recipient transgenic mice expressing the corresponding antigen in neurons. Although number and specificity of T-cells were key elements with obvious favorable CD4/CD8 T-cell interactions, Immune Checkpoint blockade was compulsory in the HA-model to obtain a PCD phenotype. A possible role for humoral activation has also been suggested in the β-Gal model, and although a dual role for B-cells in cancer progression has been shown[54], their implication in Yo-PCD should not be overlooked. Indeed, in addition to high infiltration of reactive T-cells into Yo-PCD tumors, the presence of B cells at high density and the formation of tertiary lymphoid structures is a hallmark of Yo-PCD ovarian tumors compared to non-PCD control tumor[16]. In our model, the inability of ID8 cells to trigger the production of Yo-Abs as seen in our tumor-bearing controls was compensated by active immunization against onconeural antigens CDR2 and CDR2L. However, the dissociation of the B-cell response, induced outside the tumor, from the intra-tumoral T-cells could possibly deprive our model of beneficial interactions between immune partners[55]. The question of the tumor immunogenicity is undoubtedly a central issue for modeling PND and should be able to induce both T- and B-cell activation. Genetic analysis of ovarian tumors of Yo-PCD patients shows gain in CDR2L gene[56,57] and/or mutations in either CDR2 or CDR2L[16] compared to non-PCD tumors. This genetic feature might play a role in the breakdown of immune tolerance at least for CDR2L. Therefore, overexpressed or mutated forms of Yo-antigens should be explored as a potential pathomechanism in Yo-PCD tumors. Since CDR2 and CDR2L were not found to be mutated in our implanted tumor cell line (data not shown), the use of genetically modified ID8 cells engineered in that respect or at least intra-tumoral immunization of mice with mutated Yo-antigens should be considered as an important improvement to our model in the future.

The brain environment is weakly immunogenic or immunosuppressive. In addition, the very low level of MHC class-I expressed by Purkinje cells in adults[58] protects them from a potential MHC class I-restricted immune attack[59,60]. Yet, a local secretion of IFN-γ within the CNS by CD8+ T-cells should potentially up-regulate MHC class-I expression in Purkinje cells[61], which would in turn become an easy target for onconeural antigen-specific class I-restricted CD8+ T-cells as demonstrated in previous studies using the HA model of PCD[8,59]. It could be a key mechanism to produce disease in our model; unfortunately we did not detect MHC Class-I expression by Purkinje cells in the presence of locally infiltrated parenchymal lymphocytes, suggesting an absence of secretion of IFN-γ in the brain in the early phase of infiltration. Nevertheless, the cerebral endothelium had a marked expression of MHC class-I in tumor-implanted animals which could constitute an initial mechanism and necessary condition for antigen-specific CD8 T-cells to cross the BBB. This was previously demonstrated through an antigen-dependent migration across MHC class-I expressing cerebral endothelium towards the injected cognate antigen in the CNS parenchyma[62]. Whether this process was antigen-driven in our model of Yo-PCD remains to be elucidated. At this early stage, where no MHC class-I expressing Purkinje cell was detected, there could have been no access of CD8 T-cells to intracellular Yo antigen-derived peptides. In that context, further exploration would require the presence of pro-inflammatory MHC class-I triggers in the cerebellar parenchyma to see if the infiltrated CD8 T-cells are able to induce Purkinje cell loss in an antigen-specific MHC Class-I restricted manner, and whether CDR2 and/or CDR2L are the *bona fide* targeted antigen(s). Induction of a pro-inflammatory milieu in brain parenchyma could be done in different ways. For instance, by intrathecal injection of an IFN-γ encoding adenovirus shown to induce inflammatory chemokine secretion by astrocytes and microglia and to synergize with PTX by inducing T-cell entry to the CNS[29]. Other mediators, such as Tumor Necrosis Factor (TNF), could also contribute to establishing a pro-inflammatory milieu in the CNS[63]. It could be explored as another potential mechanism in Yo-PCD neuro-inflammation using a hypersensitive mouse model to TNF, such as one deficient for A20 (TNFAIP3), shown to be very susceptible to brain inflammation and auto-immunity[64,65]. In humans, several A20 polymorphisms are associated with autoimmune pathologies[66], which could legitimate the search for key immune factors in Yo-PCD patients. Overall, only a high frequency of Ag-specific T-cells infiltrated in the cerebellar parenchyma could provoke the massive loss of antigen-bearing Purkinje cells as observed in patients, which would require a sustained inflammatory environment in the brain coupled to a strong and protracted activation in the periphery with repetitive tumor challenges.

Previously unsuccessful tolerance breakdown in early Yo-PCD models has pushed researchers to more artificial and manipulated models that can be interesting for theoretical proofs of concept but pushes us away from

more “physiological” modeling of the pathology. We have been pushing forward the strength of the immune response towards Yo-antigens CDR2 and CDR2L in our tumor-bearing models with mitigated success in brain inflammation and injury that might call for extended timing to install a self-sustained neuroinflammation. Herein, we conclude that the currently admitted Yo onconeural antigens expressed by the tumor, at least in their unmutated form, might not be the right trigger, which would legitimate the deep analysis of Yo-PCD tumors peptidome. Most likely, an essential phenotype in patients remains to be found that would point to genetic pro-inflammatory susceptibility or/and to an environmental cue in the history of patients such as a neuro-tropic virus infection[67–69]. On that account, a substantial effort should be made to explore genes and immunity of patients as we need better knowledge to model Yo-PCD that will only be drawn from translational studies.

AKNOWLEDGMENTS

CIQLE microscopy and histology platform at the SFR Lyon Est. ALECS Animal facility at Lyon 1 university. X-ray Irradiator facility at ENS Lyon.

Funding

This study is supported by research grants from Fondation pour la recherche médicale (reference DQ20170336751) and has been developed within the BETPSY project, which is supported by a public grant overseen by the French national research agency (Agence nationale de la recherche, ANR), as part of the second “Investissements d´Avenir” program (reference ANR-18-RHUS-0012). This work was supported by the French National Research Agency within the framework of the LABEX CORTEX ANR-11-LABX-0042.

Declarations

Conflict of Interest: The authors declare that they have no conflict of interest.

Data Availability: The data that support the findings of this study are available from the corresponding author upon request.

ABBREVIATIONS

Abs Antibodies

CDR Cerebellar Degeneration-Related protein

CNS Central Nervous System

FFPE Formalin-Fixed Paraffin-Embedded

IFN Interferon

MHC Major Histocompatibility complex

TNF Tumor Necrosis Factor

PCD Paraneoplastic Cerebellar Degeneration

PND Paraneoplastic Neurological Disease

PNS Paraneoplastic Neurological Syndrome

CFA Complete Freund's Adjuvant

PTX Pertussis Toxin

PBS Phosphate-Buffered Saline

SCID Severe Combined ImmunoDeficiency

TCR T-Cell Receptor

REFERENCES

1. Shams'ili, S. *et al.* Paraneoplastic cerebellar degeneration associated with antineuronal antibodies: analysis of 50 patients. *Brain* **126**, 1409–1418 (2003).
2. Verschuuren, J. *et al.* Inflammatory infiltrates and complete absence of Purkinje cells in anti-Yo-associated paraneoplastic cerebellar degeneration. *Acta Neuropathol* **91**, 519–525 (1996).
3. Yshii, L., Bost, C. & Liblau, R. Immunological Bases of Paraneoplastic Cerebellar Degeneration and Therapeutic Implications. *Front. Immunol.* **11**, (2020).

4. Tanaka, M., Tanaka, K., Onodera, O. & Tsuji, S. Trial to establish an animal model of paraneoplastic cerebellar degeneration with anti-Yo antibody. 1. Mouse strains bearing different MHC molecules produce antibodies on immunization with recombinant Yo protein, but do not cause Purkinje cell loss. *Clin Neurol Neurosurg* **97**, 95–100 (1995).
5. Tanaka, K. *et al.* Trial to establish an animal model of paraneoplastic cerebellar degeneration with anti-Yo antibody. 2. Passive transfer of murine mononuclear cells activated with recombinant Yo protein to paraneoplastic cerebellar degeneration lymphocytes in severe combined immunodeficiency mice. *Clin Neurol Neurosurg* **97**, 101–105 (1995).
6. Saiki, M. *et al.* Induction of humoral responses specific for paraneoplastic cerebellar degeneration-associated antigen by whole recombinant yeast immunization. *Journal of Autoimmunity* **24**, 203–208 (2005).
7. Sakai, K., Shirakawa, T., Kitagawa, Y., Li, Y. & Hirose, G. Induction of Cytotoxic T Lymphocytes Specific for Paraneoplastic Cerebellar Degeneration-associated Antigen in vivo by DNA Immunization. *Journal of Autoimmunity* **17**, 297–302 (2001).
8. Yshii, L. M. *et al.* CTLA4 blockade elicits paraneoplastic neurological disease in a mouse model. *Brain* **139**, 2923–2934 (2016).
9. Walker, L. S. K. & Sansom, D. M. The emerging role of CTLA4 as a cell-extrinsic regulator of T cell responses. *Nat Rev Immunol* **11**, 852–863 (2011).
10. Corradi, J. P., Yang, C., Darnell, J. C., Dalmau, J. & Darnell, R. B. A Post-Transcriptional Regulatory Mechanism Restricts Expression of the Paraneoplastic Cerebellar Degeneration Antigen cdr2 to Immune Privileged Tissues. *J. Neurosci.* **17**, 1406–1415 (1997).
11. Eichler, T. W. *et al.* CDR2L Antibodies: A New Player in Paraneoplastic Cerebellar Degeneration. *PLoS One* **8**, (2013).
12. Kråkenes, T. *et al.* CDR2L Is the Major Yo Antibody Target in Paraneoplastic Cerebellar Degeneration. *Annals of Neurology* **86**, 316–321 (2019).

13. Gebauer, C. *et al.* CD4+ and CD8+ T cells are both needed to induce paraneoplastic neurological disease in a mouse model. *OncoImmunology* **6**, e1260212 (2017).
14. Pignolet, B. S., Gebauer, C. M. & Liblau, R. S. Immunopathogenesis of paraneoplastic neurological syndromes associated with anti-Hu antibodies. *OncoImmunology* **2**, e27384 (2013).
15. Albert, M. L. *et al.* Tumor-specific killer cells in paraneoplastic cerebellar degeneration. *Nat Med* **4**, 1321–1324 (1998).
16. Small, M. *et al.* Genetic alterations and tumor immune attack in Yo paraneoplastic cerebellar degeneration. *Acta Neuropathol* **135**, 569–579 (2018).
17. Roby, K. F. *et al.* Development of a syngeneic mouse model for events related to ovarian cancer. *Carcinogenesis* **21**, 585–591 (2000).
18. Flies, D. B. & Chen, L. A simple and rapid vortex method for preparing antigen/adjuvant emulsions for immunization. *Journal of Immunological Methods* **276**, 239–242 (2003).
19. Liu, L. & Duff, K. A Technique for Serial Collection of Cerebrospinal Fluid from the Cisterna Magna in Mouse. *JoVE* 960 (2008) doi:10.3791/960.
20. Salem, M. L., Kadima, A. N., Cole, D. J. & Gillanders, W. E. Defining the antigen-specific T-cell response to vaccination and poly(I:C)/TLR3 signaling: evidence of enhanced primary and memory CD8 T-cell responses and antitumor immunity. *J Immunother* **28**, 220–228 (2005).
21. Longhi, M. P. *et al.* Dendritic cells require a systemic type I interferon response to mature and induce CD4+ Th1 immunity with poly IC as adjuvant. *J Exp Med* **206**, 1589–1602 (2009).
22. Mookerjee, A., Graciotti, M. & Kandalaft, L. E. A cancer vaccine with dendritic cells differentiated with GM-CSF and IFNα and pulsed with a squaric acid treated cell lysate improves T cell priming and tumor growth control in a mouse model. *Bioimpacts* **8**, 211–221 (2018).
23. Shibaki, A. & Katz, S. I. Induction of skewed Th1/Th2 T-cell differentiation via subcutaneous immunization with Freund's adjuvant. *Experimental Dermatology* **11**, 126–134 (2002).
24. Bennett, S. R. M. *et al.* Help for cytotoxic-T-cell responses is mediated by CD40 signalling. *Nature* **393**, 478 (1998).

25. Llopiz, D. *et al.* Combined immunization with adjuvant molecules poly(I:C) and anti-CD40 plus a tumor antigen has potent prophylactic and therapeutic antitumor effects. *Cancer Immunol Immunother* **57**, 19–29 (2008).
26. Hofstetter, H. H., Shive, C. L. & Forsthuber, T. G. Pertussis Toxin Modulates the Immune Response to Neuroantigens Injected in Incomplete Freund's Adjuvant: Induction of Th1 Cells and Experimental Autoimmune Encephalomyelitis in the Presence of High Frequencies of Th2 Cells. *J Immunol* **169**, 117–125 (2002).
27. Fujimoto, C. *et al.* Pertussis Toxin Is Superior to TLR Ligands in Enhancing Pathogenic Autoimmunity, Targeted at a Neo-Self Antigen, by Triggering Robust Expansion of Th1 Cells and Their Cytokine Production. *The Journal of Immunology* **177**, 6896–6903 (2006).
28. Cassan, C. *et al.* Pertussis Toxin Reduces the Number of Splenic Foxp3+ Regulatory T Cells. *The Journal of Immunology* **177**, 1552–1560 (2006).
29. Millward, J. M., Caruso, M., Campbell, I. L., Gauldie, J. & Owens, T. IFN-γ-Induced Chemokines Synergize with Pertussis Toxin to Promote T Cell Entry to the Central Nervous System. *The Journal of Immunology* **178**, 8175–8182 (2007).
30. Duraiswamy, J., Kaluza, K. M., Freeman, G. J. & Coukos, G. Dual Blockade of PD-1 and CTLA-4 Combined with Tumor Vaccine Effectively Restores T-Cell Rejection Function in Tumors. *Cancer Res* **73**, 3591–3603 (2013).
31. Woo, S.-R. *et al.* Immune Inhibitory Molecules LAG-3 and PD-1 Synergistically Regulate T-cell Function to Promote Tumoral Immune Escape. *Cancer Res* **72**, 917–927 (2012).
32. Joncker, N. T., Bettini, S., Boulet, D., Guiraud, M. & Guerder, S. The site of tumor development determines immunogenicity via temporal mobilization of antigen-laden dendritic cells in draining lymph nodes. *Eur. J. Immunol.* **46**, 609–618 (2016).
33. Chiang, C. L.-L., Benencia, F. & Coukos, G. Whole Tumor Antigen Vaccines. *Semin Immunol* **22**, 132–143 (2010).

34. Scheffer, S. R. *et al.* Apoptotic, but not necrotic, tumor cell vaccines induce a potent immune response in vivo. *Int J Cancer* **103**, 205–211 (2003).
35. Chiappinelli, K. B., Zahnow, C. A., Ahuja, N. & Baylin, S. B. Combining Epigenetic and Immunotherapy to Combat Cancer. *Cancer Res* **76**, 1683–1689 (2016).
36. McCaw, T. R., Randall, T. D. & Arend, R. C. Overcoming immune suppression with epigenetic modification in ovarian cancer. *Translational Research* **204**, 31–38 (2019).
37. Stone, M. L. *et al.* Epigenetic therapy activates type I interferon signaling in murine ovarian cancer to reduce immunosuppression and tumor burden. *Proc Natl Acad Sci U S A* **114**, E10981–E10990 (2017).
38. Turner, T. B. *et al.* Epigenetic modifiers upregulate MHC II and impede ovarian cancer tumor growth. *Oncotarget* **8**, 44159–44170 (2017).
39. Giometto, B. *et al.* Sub-acute cerebellar degeneration with anti-Yo autoantibodies: immunohistochemical analysis of the immune reaction in the central nervous system. *Neuropathol Appl Neurobiol* **23**, 468–474 (1997).
40. Storstein, A., Krossnes, B. K. & Vedeler, C. A. Morphological and immunohistochemical characterization of paraneoplastic cerebellar degeneration associated with Yo antibodies. *Acta Neurologica Scandinavica* **120**, 64–67 (2009).
41. Su, S. B., Silver, P. B., Zhang, M., Chan, C.-C. & Caspi, R. R. Pertussis Toxin Inhibits Induction of Tissue-Specific Autoimmune Disease by Disrupting G Protein-Coupled Signals. *The Journal of Immunology* **167**, 250–256 (2001).
42. Schläger, C. *et al.* Effector T-cell trafficking between the leptomeninges and the cerebrospinal fluid. *Nature* **530**, 349–353 (2016).
43. Maria, Z., Turner, E., Agasing, A., Kumar, G. & Axtell, R. C. Pertussis Toxin Inhibits Encephalitogenic T-Cell Infiltration and Promotes a B-Cell-Driven Disease during Th17-EAE. *International Journal of Molecular Sciences* **22**, 2924 (2021).

44. Tanaka, K. *et al.* Passive transfer and active immunization with the recombinant leucine-zipper (Yo) protein as an attempt to establish an animal model of paraneoplastic cerebellar degeneration. *Journal of the Neurological Sciences* **127**, 153–158 (1994).
45. Tanaka, M., Tanaka, K., Shinozawa, K., Idezuka, J. & Tsuji, S. Cytotoxic T cells react with recombinant Yo protein from a patient with paraneoplastic cerebellar degeneration and anti-Yo antibody. *Journal of the Neurological Sciences* **161**, 88–90 (1998).
46. Carpentier, A. F. *et al.* DNA vaccination with HuD inhibits growth of a neuroblastoma in mice. *Clin Cancer Res* **4**, 2819–2824 (1998).
47. Pellkofer, H. *et al.* Modelling paraneoplastic CNS disease: T-cells specific for the onconeuronal antigen PNMA1 mediate autoimmune encephalomyelitis in the rat. *Brain* **127**, 1822–1830 (2004).
48. Schubert, M., Panja, D., Haugen, M., Bramham, C. R. & Vedeler, C. A. Paraneoplastic CDR2 and CDR2L antibodies affect Purkinje cell calcium homeostasis. *Acta Neuropathol* **128**, 835–852 (2014).
49. Panja, D., Vedeler, C. A. & Schubert, M. Paraneoplastic cerebellar degeneration: Yo antibody alters mitochondrial calcium buffering capacity. *Neuropathology and Applied Neurobiology* **45**, 141–156 (2019).
50. Greenlee, J. E., Burns, J. B., Rose, J. W., Jaeckle, K. A. & Clawson, S. Uptake of systemically administered human anticerebellar antibody by rat Purkinje cells following blood-brain barrier disruption. *Acta Neuropathol* **89**, 341–345 (1995).
51. Graus, F. *et al.* Effect of intraventricular injection of an anti-Purkinje cell antibody (anti-Yo) in a guinea pig model. *Journal of the Neurological Sciences* **106**, 82–87 (1991).
52. Sellers, R. S. Translating Mouse Models: Immune Variation and Efficacy Testing. *Toxicol Pathol* **45**, 134–145 (2017).
53. Blachère, N. E. *et al.* T cells targeting a neuronal paraneoplastic antigen mediate tumor rejection and trigger CNS autoimmunity with humoral activation. *Eur. J. Immunol.* **44**, 3240–3251 (2014).

54. Tsou, P., Katayama, H., Ostrin, E. J. & Hanash, S. M. The Emerging Role of B Cells in Tumor Immunity. *Cancer Res* **76**, 5597–5601 (2016).
55. Shen, P. & Fillatreau, S. Antibody-independent functions of B cells: a focus on cytokines. *Nat Rev Immunol* **15**, 441–451 (2015).
56. Small, M. *et al.* Specific genetic alterations and tumor immune contexture characterize ovarian tumors with paraneoplastic degeneration and anti-Yo antibodies. *Morphologie* **101**, 245 (2017).
57. Peter, E. *et al.* Immune and Genetic Signatures of Breast Carcinomas Triggering Anti-Yo–Associated Paraneoplastic Cerebellar Degeneration. *Neurology - Neuroimmunology Neuroinflammation* **9**, (2022).
58. Lv, D. *et al.* The Similar Expression Pattern of MHC Class I Molecules in Human and Mouse Cerebellar Cortex. *Neurochem Res* **39**, 180–186 (2014).
59. Yshii, L. *et al.* IFN-γ is a therapeutic target in paraneoplastic cerebellar degeneration. *JCI Insight* **4**, (2019).
60. Cebrián, C. *et al.* MHC-I expression renders catecholaminergic neurons susceptible to T-cell-mediated degeneration. *Nat Commun* **5**, 3633 (2014).
61. Zhou, F. Molecular Mechanisms of IFN-γ to Up-Regulate MHC Class I Antigen Processing and Presentation. *International Reviews of Immunology* **28**, 239–260 (2009).
62. Galea, I. *et al.* An antigen-specific pathway for CD8 T cells across the blood-brain barrier. *J Exp Med* **204**, 2023–2030 (2007).
63. Murphy, C. A., Hoek, R. M., Wiekowski, M. T., Lira, S. A. & Sedgwick, J. D. Interactions Between Hemopoietically Derived TNF and Central Nervous System-Resident Glial Chemokines Underlie Initiation of Autoimmune Inflammation in the Brain. *The Journal of Immunology* **169**, 7054–7062 (2002).
64. Guedes, R. P. *et al.* A20 deficiency causes spontaneous neuroinflammation in mice. *Journal of Neuroinflammation* **11**, 122 (2014).

65. Catrysse, L., Vereecke, L., Beyaert, R. & van Loo, G. A20 in inflammation and autoimmunity. *Trends in Immunology* **35**, 22–31 (2014).
66. Vereecke, L., Beyaert, R. & van Loo, G. Genetic relationships between A20/TNFAIP3, chronic inflammation and autoimmune disease. *Biochemical Society Transactions* **39**, 1086–1091 (2011).
67. Münz, C., Lünemann, J. D., Getts, M. T. & Miller, S. D. Antiviral immune responses: triggers of or triggered by autoimmunity? *Nat Rev Immunol* **9**, 246–258 (2009).
68. Steinbach, K. *et al.* Brain-resident memory T cells generated early in life predispose to autoimmune disease in mice. *Science Translational Medicine* **11**, (2019).
69. Merkler, D. *et al.* "Viral déjà vu" elicits organ-specific immune disease independent of reactivity to self. *J Clin Invest* **116**, 1254–1263 (2006).

TABLE 1. Comparison of the different published models of Paraneoplastic Cerebellar Ataxia (PCA).

Antigen	Animal	Immunization	Syngeneic tumor	Adoptive transfer	Immune modulators	Results	Limitations	References
Yo	BalB/C, C3H, C57Bl/6, SJL, C57Bl/6(nu/nu) mice	Human protein CDR2 (IP), Human CDR2 DNA (gene gun) or CDR2 expressing-recombinant Yeast (SC)	No tumor	CDR2-specific activated splenocytes in SJL mice (IV, IC)	No	Auto-Abs (sera)	Non-autologous protein No tumor implanted No immunization of recipient animals	([4–7])
Hu	A/J and SWR/J mice	Human HuD DNA (IM) and protein HuD (SC)	Neuro2A cells Human Neuroblastoma (SC)	No	No	Auto-Abs (sera) Tumor regression	Immunization with non-autologous protein and non syngeneic tumor	([46])
PNMA1 (anti-Ma/Ta)	Dark Agouti (DA) rats	Rat protein PNMA1 (SC)	No tumor	PNMA1-specific CD4-T cell lines (IV)	No	Auto-Abs (sera) Immune cells in parenchyma but apoptotic	No tumor implanted No PNMA1-specific CD8-T cell transfer	([47])
β-gal (Nova2-restricted)	C57Bl/6 transgenic mice	β-gal-AdenoVirus and β-gal recombinant protein (ID)	WP4-β-gal cells Fibrosarcoma (ID)	CD4 and CD8 T-cells with β-gal -specific TCR (IV) Bone Marrow chimeras	Pertussis toxine	Auto-Abs (sera) Tumor regression Immune cells in parenchyma Neuronal loss Ataxia or death (25% of mice)	Neuro-antigen unrelated to PCA High density T-cells required for pathogenicity	([53])
HA * (Purkinje cell-specific)	BalB/C transgenic mice	No	4T1- HA cells Breast cancer (SC)	CD4 and CD8 T-cells with HA-specific TCR (IV)	anti-CTLA-4	Auto-Abs (sera) Tumor regression Immune cells in parenchyma Neuronal loss Ataxia	Neuro-antigen unrelated to PCA High density T-cells required for pathogenicity	([8])
Yo	C57Bl/6 mice	Recombinant protein CDR2 and CDR2L (SC) ID8 cell lysate	ID8 cells Ovarian carcinoma (SC)	No	anti-CTLA-4 anti-PD-1 Pertussis toxine anti-CD40 HDACi, DNMTi	Auto-Abs (sera, CSF) Tumor regression Immune cells in parenchyma Heterogeneous neuronal loss	Low density cerebellar T-cells in parenchyma Prolonged timing might be required for pathogenicity	Our study

**Transmembrane antigen where others are intracellular. IC: intracerebral, ID: intradermic, IM: intramuscular, IP: intraperitoneal, IV: intravenous, SC: subcutaneous.*

***Figure 1*: Experimental designs for Yo-PCD modeling in mouse showing chronology of ID8 cells implantation and immunization schemes.** *5.10^6 ID8 cells (red arrow) were implanted intraperitoneally **(A-B-C)** or subcutaneously **(D)** prior to immunization (blue arrows) **(A-B)** or after immunization **(C-D)**. Tables show immunization scheme and adjuvants used on injection days also annotated by blue arrows on timeline. Long term treatments such as ICIs and epigenetic inhibitors entinostat (HDACi) and 5-azacytidine (DNMTi) are indicated as an arrow below weekly annotated timeline and dotted arrow when half dosed. End of experiment is indicated by a red cross.*

***Figure 2*: ID8 cells in vitro phenotype, and in vivo tumor growth in IP-implanted mice.**

*(**A**) Expression of CDR2 and CDR2L by ID8 cells. IF staining with CSF from patient (left), anti-CDR2L antibody (middle) and anti-CDR2 antibody (right) and their respective negative controls. (**B**) PD-L1 in vitro expression of ID8 cells was assessed by flow cytometry in the absence or presence of 75ng/mL IFN-γ (blue curve) compared to isotype control (red curve). (**C**) Representative images of tumor invasion of the diaphragm (top) and peritoneum (bottom) at end-point and HPS histological staining of corresponding PFA-fixed biopsies showing a dense and cellular tumor formation.*

***Figure 3*: Autoantibodies against CDR2 and CDR2L are present in serum and CSF of immunized mice.**

*Representative CBA in HEK cells (40x magnification) transfected with either GFP-tagged CDR2 or CDR2L. Immunostaining was done with (**A**) Serum or (**B**) CSF from representative immunized ICI-treated ID8 cell implanted mouse #PD-1 (Immunized ID8-bearing**)** and non-immunized ID8 cell implanted control mouse #ID-2 (ID8-bearing). Autoantibodies were revealed with anti-mouse IgG coupled with A647. Overlapping signals (red and green) confirm the presence of autoantibodies against CDR2 and CDR2L in samples from immunized mice but not from tumor-bearing control mice. (**C**) Immunostaining of rat cerebellar slices with serum from an immunized and tumor implanted mouse (left), versus with serum from a littermate mouse (right).*

***Figure 4*: Subcutaneous implantation of ID8 cells triggers immune infiltration in the brain.**

***(A)** Tumor growth in ID8 s.c implanted hosts immunized (ID8vax) or not (ID8) was assessed every week (mean±SEM, n=6 mice). Repeated measure two-way ANOVA and Sidak post-test (week2: p=0.0024, week6: p=0.0388). **(B-C-E)** Littermate mice (WT), immunized (ID8vax sc, ID8vax IP) or not (ID8 sc) tumor-bearing mice (mean±SEM, n=6 mice per group) analyzed using Kruskal wallis test and Dunn's post-test. (**B**) Spleen weight measured at end-point. (**C**) Purkinje cell density measured in Vermis and Hemisphere regions of the cerebellum.*

*(**D**) Immunohistological analysis of cerebellar hemisphere from a tumor-bearing mouse showing staining of $CD3^+$, and $CD8^+$ cells in brown indicated by red arrows in the parenchyma (top), perivascular zone (middle) or choroïd plexus (bottom), and contact with Purkinje cells indicated by a black arrow. (**E**) Quantitative evaluation of total $CD3^+$ and $CD8^+$ cells in corresponding brain slices from subcutaneously-implanted (sc) groups compared to intraperitoneally-implanted (IP) immunized mice (n=6), and (**F**) quantification of $CD3^+$ and $CD8^+$ cells in parenchyma of cerebellar hemisphere. (**G**) Immunohistological analysis of cerebellar hemisphere from a tumor-bearing mouse showing MHC Class-I staining in brown: Purkinje cells (black arrows) in parenchyma showing no staining (top), endothelial barrier (middle), and Choroïd plexus (bottom). *p<0.05;**p<0.01;***<0.0001.*

***Figure 1**: Experimental designs for Yo-PCD modeling in mouse showing chronology of ID8 cells implantation and immunization schemes.*

A

Immunization	
CDR2 + CDR2L	
D30	D42
poly IC	poly IC

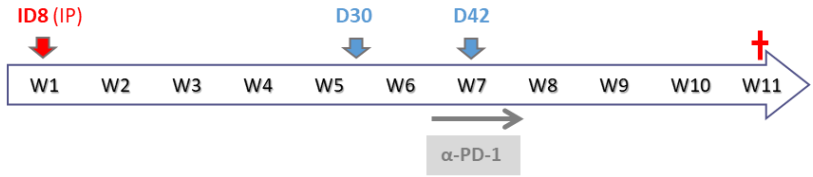

B

Immunization		
CDR2 + CDR2L		
D7	D18	D42
poly IC	poly IC	poly IC

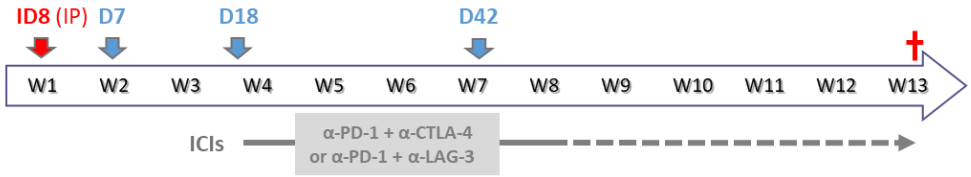

C

Immunization		
CDR2 + CDR2L + necrotic ID8 lysate		
D0	D13	D35
CFA	poly IC	poly IC
anti-CD40	anti-CD40	PTX

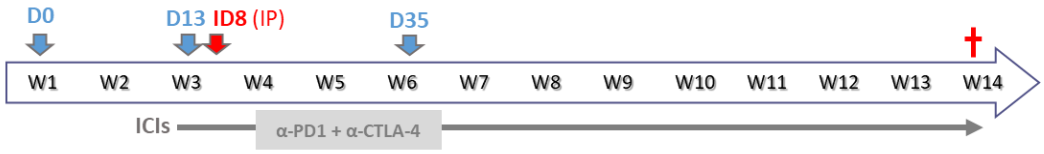

D

Immunization		
CDR2 + CDR2L necrotic+apoptotic ID8 lysate		
D0	D13	D35
CFA	PTX	PTX
anti-CD40	anti-CD40	anti-CD40
poly IC	poly IC	poly IC

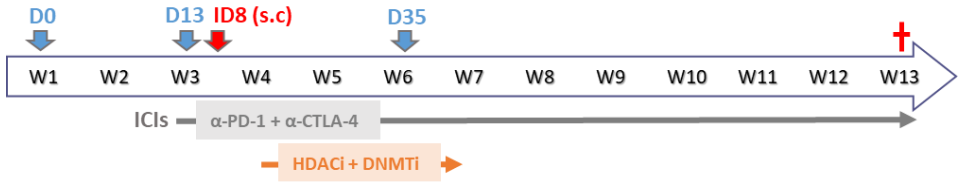

***Figure 2*: ID8 cells in vitro phenotype, and in vivo tumor growth in IP-implanted model.**

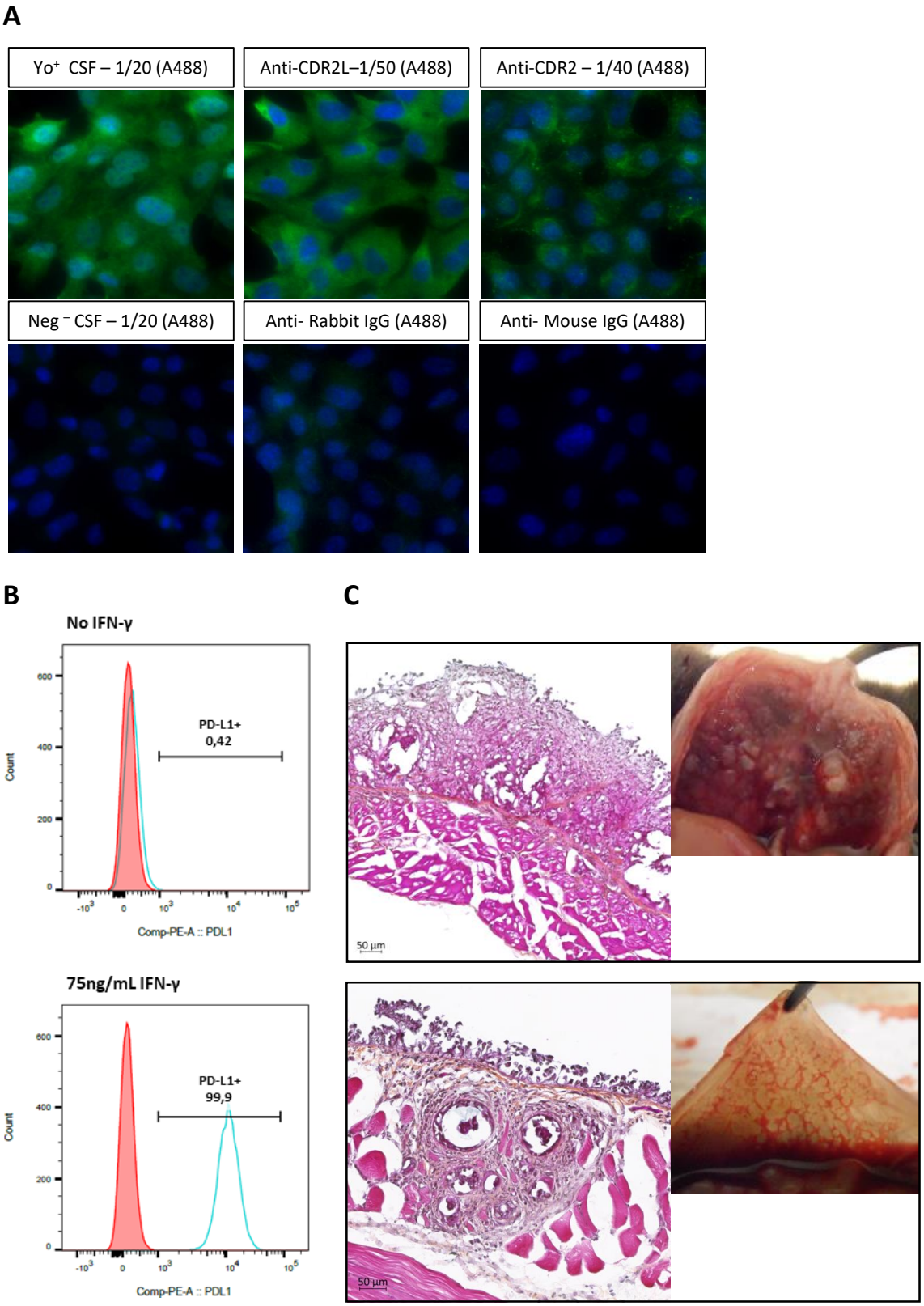

***Figure 3*: Autoantibodies against CDR2 and CDR2L are present in serum and CSF of immunized mice, and autoantibody-containing serum labels Purkinje cells.**

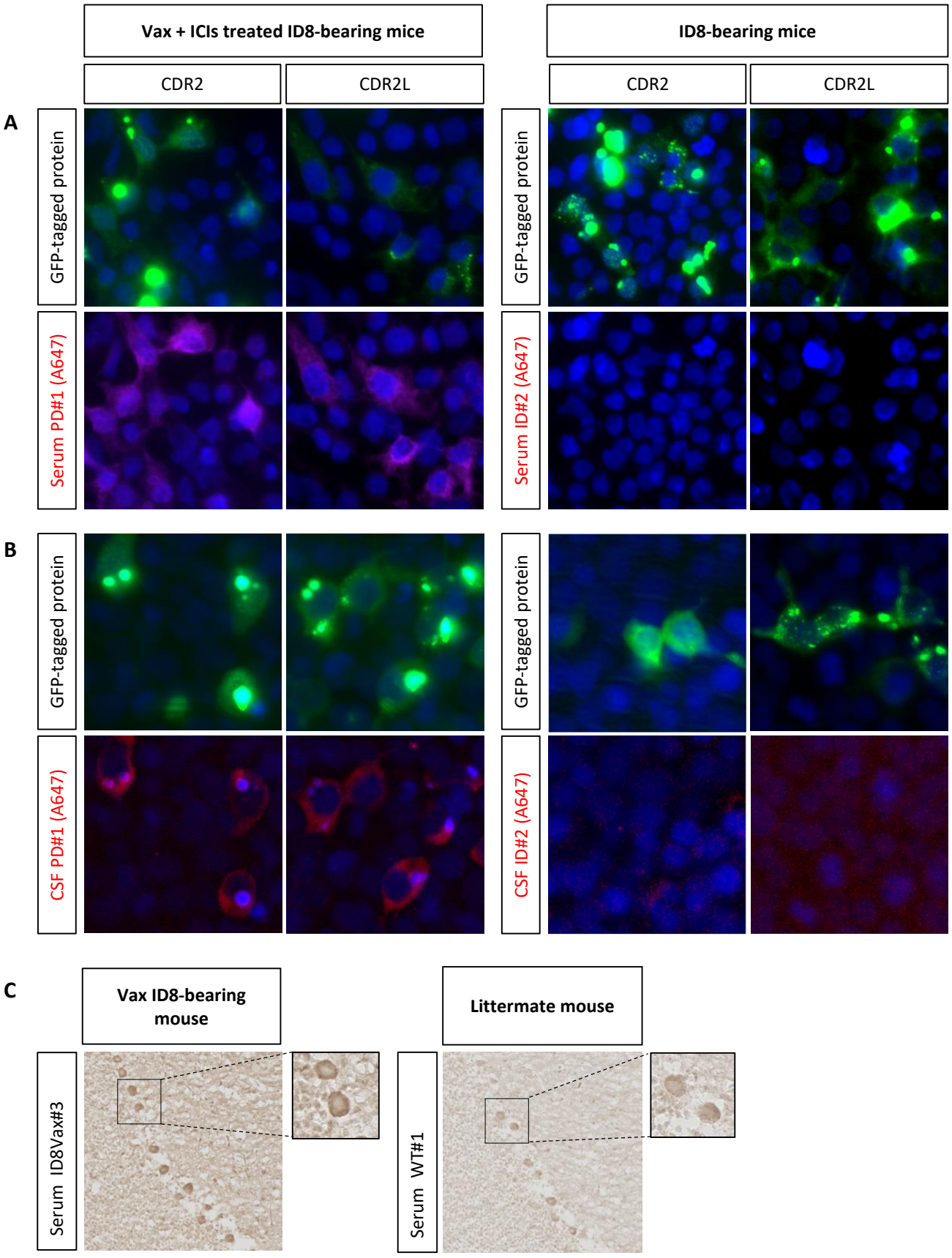

***Figure 4*: Subcutaneous implantation of ID8 cells triggers immune infiltration in the brain.**